

Raman study of optical phonons in ultrathin InAs/InP single strained quantum wells

A. Lanacer,* J. F. Chabot, M. Côté, and R. Leonelli

Département de Physique and Regroupement, Québécois sur les Matériaux de Pointe (RQMP), Université de Montréal, Case Postale 6128, Succursale Centre-ville, Montréal, Québec, H3C 3J7 Canada

D. Frankland and R. A. Masut†

Département de Génie Physique and Regroupement Québécois sur les matériaux de pointe (RQMP), École Polytechnique, Case Postale 6079, Succursale Centre-ville, Montréal, Québec, H3C 3A7 Canada

(Received 20 April 2005; revised manuscript received 6 July 2005; published 19 August 2005)

By means of Raman scattering, photoluminescence, and x-ray diffraction experiments, we have studied a series of ultrathin InAs/InP single quantum wells grown with nominal well thickness varying between one and four monolayers. The observed Raman peaks are attributed to the first InAs-confined longitudinal optical phonon. When the quantum well is thinner than three monolayers, the measured frequencies of the confined modes depart from the predictions of the standard confined-phonon model but are in good agreement with the results of *ab initio* calculations based on density-functional theory. This indicates that there is a significant penetration of the InAs layer vibrations in the InP barriers and that thickness fluctuations occur at a scale short enough to further shift the phonon frequencies. When the wells contain more than three monolayers, a doublet Raman structure is observed which parallels the evolution of the photoluminescence spectra from single- to multiple-peak emission. We associate this simultaneous change in Raman and photoluminescence spectra with the two- to three-dimensional growth-mode transition.

DOI: [10.1103/PhysRevB.72.075349](https://doi.org/10.1103/PhysRevB.72.075349)

PACS number(s): 63.22.+m, 78.67.De, 71.15.Mb, 78.30.-j

I. INTRODUCTION

Low-dimensional semiconductor heterostructures have revealed new physical phenomena at a quantum scale through fundamental studies and as a consequence have important applications in high-speed electronics and optoelectronics.¹ In particular, systems based on InAs and InP with a lattice mismatch of 3.2% have significant potential for long-wavelength optoelectronic device applications.²⁻⁴ For example, lasing at the 1.55- μm optical fiber telecommunication wavelength has been achieved using InAs quantum dots (QD's) grown on InP substrates in the Stranski-Krastanov mode.⁵ The well-established progress in epitaxial growth techniques now allows the controlled growth of quantum wells (QW's) as thin as one monolayer (ML). Such a control is required since, in the case of the InAs/InP system, the transition between pseudomorphic [two dimensional (2D)] and Stranski-Krastanov (3D) growth modes occurs at InAs thicknesses between 1 and 5 ML, depending on growth conditions.⁶ Decreasing to this scale the layer practically merges with the interface whose morphology plays an increasingly important role in the optical and electronic properties of the heterostructure.^{7,8}

In the specific case of the InAs/InP system, a multicomponent photoluminescence (PL) spectrum is observed when the deposited amount of InAs exceeds a value which is close to the 2D-3D growth-mode transition. The different PL components are associated with either strained QW's (Ref. 9) or relaxed elongated islands⁶ with monolayer fluctuations in height.

For InAs/InP QW's, where the dispersion curves of the optical phonons of the two constituent materials do not overlap, the vibrations generated into the well cannot propagate into the barrier and the phonons are practically confined in

the well material. This confinement results in a shift towards lower frequencies of the longitudinal optical (LO) modes. Additionally, the frequency shifts to higher (lower) energies when the layer is subjected to a compressive (tensile) strain, respectively.¹⁰ Vibrational modes such as those of the LO branch are very sensitive to the nature and roughness of the interface. This fact makes Raman and PL spectroscopies powerful and complementary tools to investigate the structural and electronic properties of thin-layer heterostructure systems.

The observation of confined LO modes has been reported in several Raman studies on superlattices and single QW's since the early 1980s.^{10,11} Within the usual confined-phonon model,¹² there are N confined LO modes in a well which consists of N monolayers. The frequencies of these modes are near that of the LO phonons of the bulk crystal with wave vector k_m given by

$$k_m = \frac{m\pi}{(N + \delta)a}, \quad (1)$$

where $m(1 \leq m \leq N)$ is an integer, a is the monolayer thickness, and δ is an adjustable parameter usually taken close to 1 which accounts for the penetration of the vibration into the barriers. Yet the observation of confined optical phonons in InAs/InP ultrathin single quantum wells (SQW's) is rather limited¹³⁻¹⁶ and a considerable fraction applies to samples grown by atomic layer epitaxy at low temperatures (near 350 °C). These samples have sharp, well-defined interfaces with hardly any interdiffusion, but rather poor nonoptimized optical properties and hence no clear PL spectra available.

In this paper we present a photoluminescence and Raman scattering study of ultrathin InAs/InP SQW's grown by low-

pressure metalorganic vapor-phase epitaxy. The Raman signal from the first confined LO mode is observed in samples with InAs thicknesses as small as 1.3 ML. The frequency of this mode follows the predictions of *ab initio* calculations, a clear indication that short-scale interface roughness results in a continuous shift with layer thickness of the confined phonon frequency. We also find that Raman scattering is sensitive to the 2D-3D growth-mode transition which, for our samples, occurs at a thickness close to 2.4 ML.

II. EXPERIMENTS

A series of InAs SQW's in InP were grown by low-pressure metalorganic vapor-phase epitaxy (MOVPE). The growth procedure consists in the deposition of a 100-nm InP buffer layer on Fe-doped (100) semi-insulating InP substrates, followed by several InAs monolayers and terminated by the deposition of a 30-nm InP cap layer. The growth apparatus is equipped with a fast-switching gas manifold, and all the valves are computer controlled. More details on this experimental equipment are given elsewhere.¹⁷ Trimethylindium (TMI), tertiarybutylarsine (TBA), and tertiarybutylphosphine (TBP) were used as precursors and Pd-purified H₂ as the carrier gas. During the growth of all the samples the substrate temperature was kept at 600 °C for both the InP buffer and the cap layer and the reactor pressure was 160 Torr. For the InAs layer, the growth temperature was previously lowered from 600 to 500 °C during 90 s where approximately 20 ML of InP were grown at 500 °C. A growth interruption sequence, optimized for this combination of materials, was used to switch from barrier to well layer and vice versa.¹⁸

The Raman measurements were performed at room temperature in the backscattering geometry. Parallel $z(x,x)\bar{z}$ and crossed $z(x,y)\bar{z}$ polarization configurations were used, where the z axis is parallel to the [001] growth axis, while x and y are in the layer plane and correspond to the [100] and [010] axes, respectively. The samples were excited by the 514.5-nm line of an argon-ion laser with a power density of 100 W/cm². To avoid light scattering by air the samples were kept under helium atmosphere. The scattered light was dispersed by a 1-m double spectrometer and detected by a liquid-nitrogen-cooled Si charge coupled device. The typical time of acquisition was 60 min. The resolution of the spectroscopic system was set at 1 cm⁻¹. To achieve absolute wave number calibration and to correct for small drifts during the motion of the spectrometer, plasma lines of the Ar-ion laser, present on the recorded spectra, have been used. For the PL measurements, the samples were mounted strain free in a helium flow cryostat and cooled to 6 K. The excitation source was the 632.8-nm line of a He—Ne laser with a power output of 15 mW. The signal was detected by liquid-nitrogen-cooled InGaAs and InSb detectors and analyzed with a BOMEM Fourier transform spectrometer.

Triple-axis high-resolution x-ray diffraction (HR-XRD) ω - 2θ (004) scans were performed in order to determine the layer thicknesses and overall crystal quality. The instrument used was a Philips HRD diffractometer with a triple-axis detector and a four-crystal monochromator in Ge(220) mode.

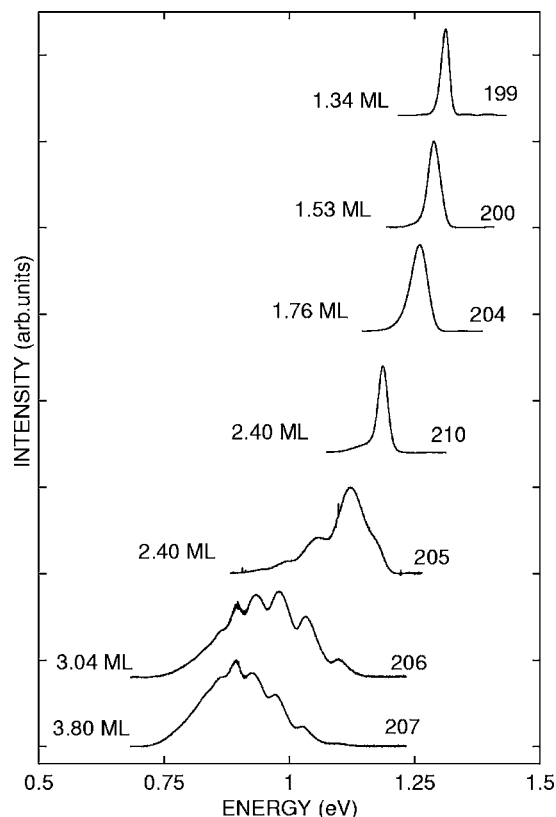


FIG. 1. PL spectra taken at 6 K for InAs/InP QW's. The numbers at the left side are the InAs slab thickness measured by HR-XRD.

When compared with the more standard five-crystal (receiving slit) configuration, the triple-axis configuration, which involves seven crystals, significantly improves the angular resolution around Bragg peaks. This is especially important in the case of single ultrathin layers for which the structural information is found near substrate Bragg peaks.

III. RESULTS

The InAs thickness d_{XRD} of the SQW's was determined by simulating the HR-XRD scans with the Tagaki-Taupin equations of the dynamical diffraction theory.¹⁹ The simulations assumed that the layers are pseudomorphic with the InP substrate and that continuum elasticity theory applies. HR-XRD spectra of fully strained samples give an average of the QW materials and are not very sensitive to the morphology of the interface. On the other hand, PL spectra are very sensitive to microscopic potential fluctuations which localize the excitons before they recombine, resulting in a Stokes shift between absorption and emission.¹⁸

The evolution of the PL spectra of the samples as a function of InAs thickness is depicted in Fig. 1. The samples can be separated in two groups according to the shape of their PL spectra. The first group has single-peak PL spectra with full width at half maximum (FWHM) between 19 and 46 meV. The second group is characterized by multicomponent PL spectra. Following Gendry *et al.*,⁶ we tentatively associate

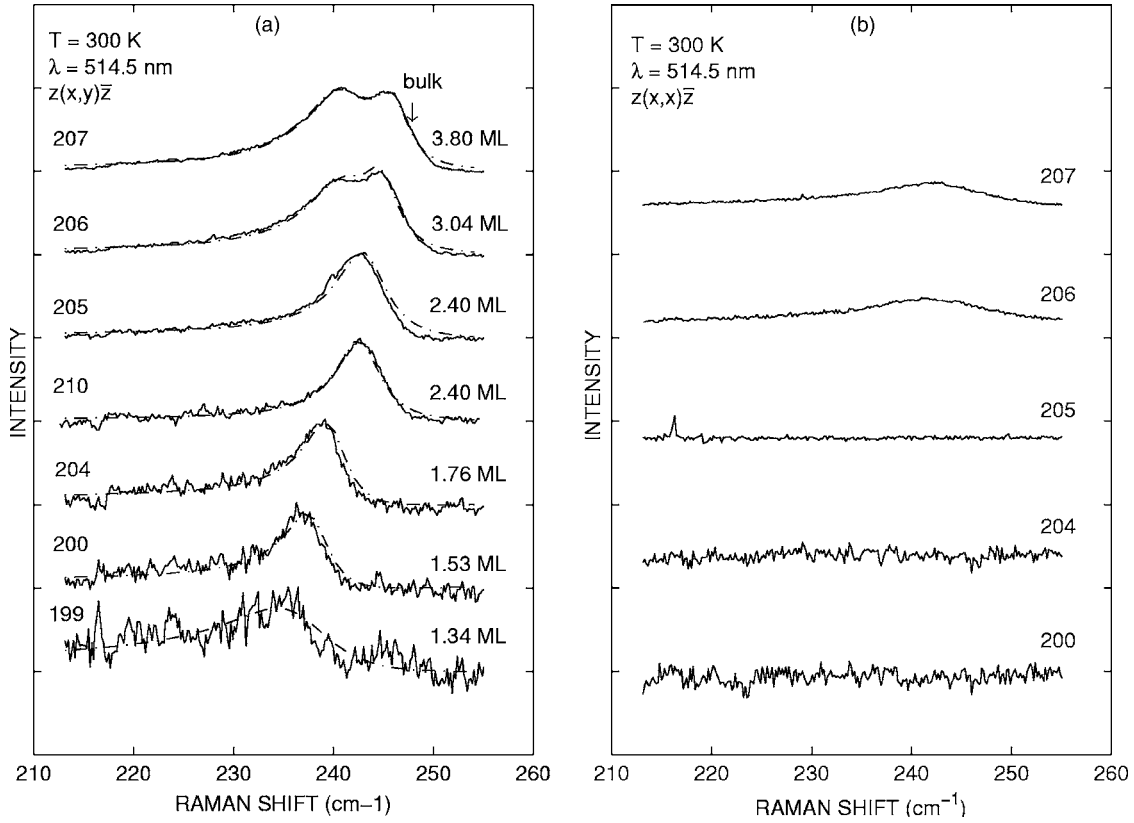


FIG. 2. Room-temperature Raman spectra of the different samples. The excitation wavelength was 514.5 nm, and the spectra were recorded in (a) $z(x,y)\bar{z}$ and (b) $z(x,x)\bar{z}$ configurations. The dashed lines in (a) are the Breit-Wigner-Fano fit using Eq. (2) and the parameters listed in Table I.

the appearance of a multiplex emission with the 2D-3D growth-mode transition which occurs, under our growth conditions, at a thickness close to 2.4 ML.

Raman spectra were obtained from all samples in both the $z(x,y)\bar{z}$ and $z(x,x)\bar{z}$ configurations. The raw data were treated as follows: the spectra were normalized by taking a spectra of an InP(001) substrate under the same conditions in the $z(x,y)\bar{z}$ configuration. The intensity of the InP LO mode then corresponds to a normalization factor which was applied to the Raman spectra of all samples. The contribution to the Raman spectra from the InAs slabs was obtained by subtracting the Raman spectrum of the InP substrate from that of the InAs/InP samples. Figure 2 shows the resulting Raman spectra in the frequency range for InAs vibrations. The common feature of the spectra from samples with InAs thickness less than 3 ML is the presence of a single asymmetric peak in the $z(x,y)\bar{z}$ configuration while no signal is measured in the $z(x,x)\bar{z}$ one. For the two samples with $d_{XRD} > 3$ ML, two-component spectra are obtained in the $z(x,y)\bar{z}$ geometry and a much weaker structure is detected in the $z(x,x)\bar{z}$ geometry.

In order to further quantify these measurements, we fitted the spectra with Fano line shapes. Asymmetric Fano line shapes, which originate from electron-LO-phonon coupling, have already been observed in the Raman spectra of semiconductor QW structures.²⁰⁻²³ Indeed, if the continuum of the electronic intrasubband transitions overlaps the discrete phonon state, a Fano-type interaction between electrons and

phonons takes place and the Raman line shape becomes asymmetric. In this case the intensity profile of the Raman spectrum can be written as²⁴

$$I(\omega) = I_0 \frac{[1 + (\omega - \omega_{BWF})/q\Gamma]^2}{1 + [(\omega - \omega_{BWF})/\Gamma]^2}, \quad (2)$$

where $1/q$ is a measure of the interaction between the phonon and electronic state continuum, Γ is the peak broadening, and ω_{BWF} is the Breit-Wigner-Fano (BWF) peak frequency at maximum intensity I_0 . As can be seen in Fig. 2, Eq. (2) describes the experimental data very well. The optimized BWF parameters for the Raman peaks are given in Table I. Larger absolute values of $1/q$ are measured in samples with $d < 2$ ML. This is an expected result since these samples contain thinner SQW's and hence the overlap between the discrete and continuum states is stronger.

IV. ANALYSIS OF THE RESULTS

In Raman backscattering experiments, only optical phonons with wave vector $k||z$ ($k_z \neq 0$, $k_x = k_y = 0$) are probed if wave vector conservation does not break down. Within the standard confined-phonon model, the energies of the confined LO modes are given by those of the bulk material calculated at a wave vector given by Eq. (1). For even or odd mode index m , the LO modes belong to the A_1 or B_2 symmetry of the D_{2d} point group of the QW, respectively. The

TABLE I. HR-XRD InAs thickness and the optimized BWF line shape parameters of the observed Raman peaks for the samples studied in this work.

Sample	$d_{XRD} \pm 0.15$ (ML)	ω_{BWF} (cm^{-1})	$1/q$	Γ (cm^{-1})
InAs199	1.34	236.7	-0.37	6.3
InAs200	1.53	238.1	-0.29	2.6
InAs204	1.76	239.9	-0.26	2.5
InAs210	2.40	242.8	-0.10	2.6
InAs205	2.40	243.3	-0.15	3.0
InAs206	3.04	245.0	-0.12	2.0
	—	241.0	-0.12	4.0
InAs207	3.80	246.1	-0.13	2.0
	—	240.7	-0.13	4.0
ALE32	6.00	247.1	—	1.8

Raman tensors for A_1 and B_2 phonons with respect to the (x, y, z) crystal axes with $x=[100]$, $y=[010]$, and $z=[001]$ are given by²⁵

$$T_{A_1} = \begin{pmatrix} a & 0 & 0 \\ 0 & a & 0 \\ 0 & 0 & b \end{pmatrix}, \quad T_{B_2} = \begin{pmatrix} 0 & d & 0 \\ d & 0 & 0 \\ 0 & 0 & 0 \end{pmatrix}. \quad (3)$$

It follows that phonons with B_2 symmetry, which couple to electrons via the deformation potential interaction, are observed in the depolarized $z(x, y)\bar{z}$ configuration while A_1 phonons, which are induced by the Fröhlich interaction, are present in the $z(x, x)\bar{z}$ scattering configuration.²⁶ Since for our experiments the excitation energy is far from any electronic resonance of the InAs SQW's, the scattering cross section for A_1 phonons (m even) is much smaller than that for B_2 phonons (m odd).^{27,28} Moreover, the Raman intensity of the confined phonon modes decreases with the mode index²⁹ approximately as $1/m^2$. This explains why a single Fano line shape is sufficient to model the spectra shown in Fig. 2 for samples with $d_{XRD} < 2.4$ ML. The deduced phonon frequency can thus be assigned to the confined phonon LO_1 of index $m=1$. Further interpretation of the Raman results using Eq. (1) is, however, difficult because neither the LO phonon dispersion for unstrained bulk InAs nor the effect of biaxial strain on it is accurately determined.

In order to circumvent this problem, an *ab initio* method based on the density-functional theory^{31,32} (DFT) was used to calculate the phonon spectrum of InAs SQW's in InP. We used the ABINIT code^{33,34} to calculate the ground-state energy and the phonon eigenvalues and their displacement vectors. The exchange-correlation functional within the local density approximation (LDA) was employed.³⁵ For each of the three elements (In, As, and P) we used pseudopotentials generated following the method of Trouillier and Martin³⁶ in order to integrate the effects of the core electrons. The valence electrons are included explicitly. The electronic wave function is described by a plane-wave basis up to an energy cutoff of 24 hartrees. A dense k -point shifted Monkhorst-Pack

TABLE II. Experimental and calculated lattice parameters and Poisson coefficients of InAs and InP materials.

	a_{InAs} (Å)	a_{InP} (Å)	c_{InAs} (Å)	C_{12}/C_{11}
Expt	6.04	5.87	6.22	0.544 ^a
<i>Ab initio</i>	5.96	5.78	6.16	0.559

^aObtained from Ref. 30.

$8 \times 8 \times 8$ grid,^{37,38} which guarantees a convergence to better than 0.5 mhartree/atom, was used to sample the electronic states in the Brillouin zone. We used the Broyden-Fletcher-Goldfarb-Shanno (BFGS) minimization³⁹ for the structural optimization. A linear response scheme^{40,41} was also performed to get the phonon dispersion curves for bulk strained InAs with a q -point nonshifted grid of $4 \times 4 \times 4$. The main results of the calculation are summarized in Table II and Fig. 3.

In Table II we have listed the calculated and experimental lattice parameters of the bulk structure (fcc) for the InP and InAs materials. We find good agreement between experimental and calculated parameters, the difference being of the order of 1.5% and 1.3% for InP and InAs, respectively. The calculated values are slightly smaller as compared to the experimental data, which is typical of the LDA functional used.

To calculate the c_{InAs} parameter for the strained bulk InAs structure we used the calculated a_{InP} lattice parameter for the InAs xy -plane lattice parameter. The value of $c_{\text{InAs}}=6.16$ Å was found which is an expected result since the InAs lattice is subjected to compressive strain and hence the unit cell is tetragonally distorted. The ratio C_{12}/C_{11} between the elastic moduli of InAs was drawn from the expression

$$c_{\text{InAs}} = -2C_{12}/C_{11}[a_{\text{InP}} - a_{\text{InAs}}] + a_{\text{InAs}}. \quad (4)$$

The calculated value $C_{12}/C_{11}=0.559$ is 2.5% higher than the value reported in the literature, which demonstrates the good agreement between the calculations and the experimental data.

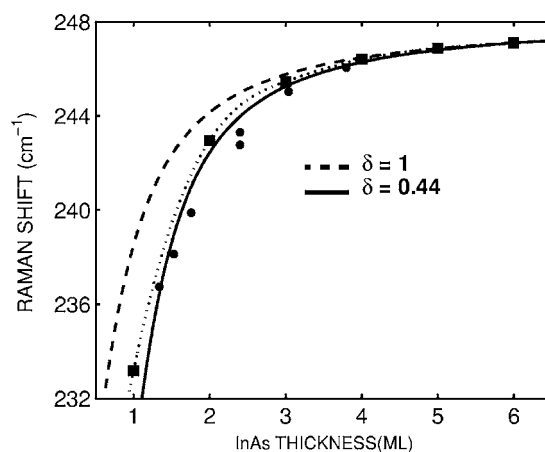


FIG. 3. Energy position of the LO_1 confined modes as a function of well thickness. Dots: measured data. Squares: *ab initio* calculation. Solid and dashed curves: frequencies obtained from Eq. (1) with $\delta=0.44$ and 1.

Figure 3 shows the calculated frequencies of the confined LO_1 phonon modes for InAs slabs ranging from 1 to 6 ML in thickness. Since the phonon frequencies obtained depend on the lattice parameter used in the calculation, the in-plane lattice parameter of the slabs was fixed at the experimental InP value—e.g., $a_{||}=5.87$ Å—in order to better compare to experimental results. However, there are still small differences between calculated values and experimental data which can be attributed to temperature effects and the inherent accuracy of the method. For this reason, the calculated frequencies were further normalized by a constant factor (≈ 0.94) to achieve agreement with the observed LO_1 frequency in sample ALE32, which has a well-controlled thickness of 6 ML. Figure 3 also shows the measured frequencies of the LO_1 phonons for our SQW samples. The agreement between the measurements and frequencies obtained by interpolating the calculated ones is rather good even though, for thinner QW's ($d_{XRD} < 3$ ML), the observed frequency is somewhat lower than the interpolated one. This difference possibly comes from a diffusion of phosphorus in the InAs layer during the growth process. Indeed, $InAs_{1-x}P_x$ alloys displays a two-mode behavior of the LO phonon over the whole composition range⁴² and the LO frequency of the InAs mode decreases slightly with increasing P concentration. Obviously, the effect of some As—P intermixing would be more pronounced for the thinner layers.

In order to connect with the more standard confined-phonon model, the LO-phonon dispersion curve of bulk strained InAs in the Γ - L direction was also calculated with the *ab initio* method. The confined phonon frequencies obtained from Eq. (1) and evaluated at the experimental lattice parameters are also shown on Fig. 3 for different values of the parameter δ . As can be seen, a value of $\delta=0.44$ reproduces well the experimental data while the value of $\delta=1$ usually assumed in superlattices is clearly inadequate. Within a classical linear-chain calculation, a value of $\delta=1$ implies a vanishing penetration length of the InAs slab vibrations into the InP matrix and thus a pinning of the first phosphorus atoms next to the InAs slab.¹² In contrast, our *ab initio* calculations show that for the LO_1 mode, the first neighboring P atoms move in antiphase with the As atoms as can be seen in Fig. 4. This result can be understood by considering which modes within InP couple to the InAs Γ_{LO} mode. Since the InAs Γ_{LO} mode is within the energy gap between the acoustic and optical modes of the phonon spectrum of the InP compound, the phonon modes which are closest in energy in the InP region are those at the X point of the Brillouin zone. These modes require that atoms in adjacent cell move in opposite directions. Hence, because of the matching condition between the two regions, the wave amplitude cancels inside the QW rather than at the phosphorus atom position. This corresponds to a value of δ less than 1. It should also be pointed out that Eq. (1) comes from a continuum model where purely mechanical boundary conditions are used. When there is no significant penetration of the vibration of the well into the barriers ($\delta \sim 1$), these boundary conditions hold well. However, a more complete continuum model must also include the continuity of the electric potential and the normal component of the electric field at the interfaces.^{43,44}

Another result of our study is that the frequency of the confined LO_1 modes varies continuously between the dis-

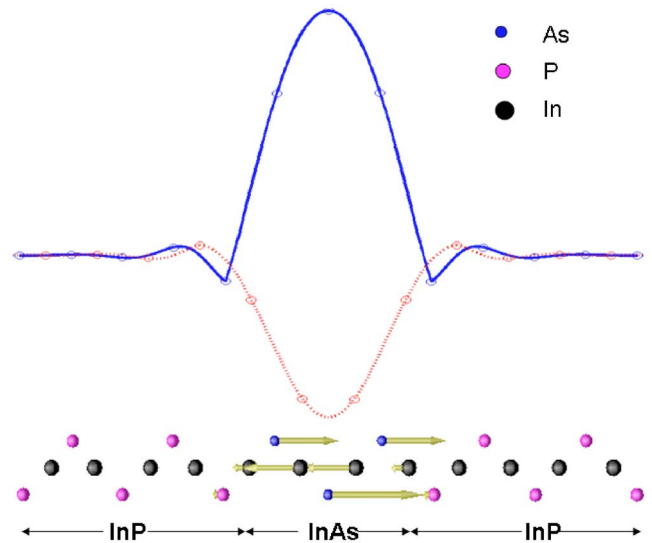


FIG. 4. (Color online) Motion of the atoms of the LO_1 mode as determined by our *ab initio* calculations. The solid line in the upper part of the figure represents the displacement of the As/P atoms and the dotted line the displacement of the In atoms. In the lower part of the figure, the displacement of the atoms is represented by arrows.

crete values corresponding to perfect InAs slabs. The observed frequencies are not some weighted average of these discrete values since the phonon broadening Γ remains small for all but the thinnest layer. For example, for sample 200 ($d_{XRD}=1.5$ ML), $\Gamma=2.6$ cm^{-1} , a value much smaller than the calculated frequency difference of 10 cm^{-1} between the 1- and 2-ML slabs. Furthermore, the excellent agreement between calculated and measured frequencies shows that the Raman scattering process performs a macroscopic average similar to that obtained by HR-XRD spectra. The continuous LO_1 frequency shift can therefore be attributed to lateral confinement of the phonons which arises from short-scale fluctuations of the InAs layer thickness. Although the actual extent of these fluctuations is difficult to quantify, some indications can be obtained from valence force field calculations of the phonon modes in InAs spheres.⁴⁵ Significant size-induced frequency shifts were obtained for sphere diameters up to 6 nm.

Finally, let us discuss the appearance of a doublet structure for the samples where $d_{XRD} \geq 3$ ML. Similar spectra were reported in Ref. 16. The low-frequency component of the doublet was attributed to a combination of interface modes and vibrations within an intermixed InAsP layer. However, in our case, the Raman doublets appear in the samples where a pronounced multicomponent PL spectrum is observed. We thus attribute the presence of the doublet Raman structure to the onset of the 2D-3D growth-mode transition. Above this transition, regions with strained SQW's 3 or 4 ML thick would then coexist with regions where relaxed nanostructures such as quantum wires with monolayer height variations would prevail.⁴⁶ The low-frequency component of the doublet, at ~ 241 cm^{-1} , can then be explained by the presence of an InAs wetting layer with a thickness close to 2 ML associated with the relaxed nanostructures.

V. CONCLUSIONS

We have investigated by Raman spectroscopy the confined phonon modes of single InAs quantum wells in InP with well thickness between 1.3 and 3.8 monolayers. For samples with thicknesses smaller than 3 ML, a single Raman peak with a Fano line shape is observed in the InAs-like frequency range. From symmetry considerations, we attribute this peak to the first InAs-confined LO phonon. The frequency of this phonon varies continuously with InAs thickness rather than taking on only discrete values. The frequency variation with thickness departs from the predictions of the simple continuum model of confined phonons standard confined-phonon model; it is, however, in excellent agreement with an *ab initio* calculation for strained InAs quantum wells in InP. This indicates that there is a significant penetration of the InAs layer vibrations in the InP barriers together with lateral phonon confinement induced by short-scale InAs layer thickness fluctuations.

When the thickness of the InAs wells is increased beyond 3 ML, a doublet Raman structure appears. In parallel, the photoluminescence spectra evolve from a single peak to a

multicomponent emission. We attribute this more complex Raman spectrum to the coexistence of regions with strained quantum wells with others where relaxed nanostructures have grown on a 2-ML-thick InAs wetting layer in the Stranski-Krastanov growth mode. Our study shows that even a macroscopic probe such as Raman scattering can provide precise quantitative information on the microscopic morphology of ultrathin heterostructures.

ACKNOWLEDGMENTS

This work was supported by the Natural Sciences and Engineering Research Council of Canada (NSERC), the Fonds Québécois de la Recherche sur la Nature et les Technologies (FQRNT), and the Réseau Québécois de Recherche en Nanosciences et Nanotechnologies (NanoQuébec). The computational resources were provided by the Réseau Québécois de Calcul de Haute Performance (RQCHP). One of the authors (R.A.M.) acknowledges financial assistance under Grant No. SAB2003-0159 from the Ministerio de Educación y Ciencia of Spain for a sabbatical period during which part of this work was completed.

*Electronic address: ali.lanacer@umontreal.ca

[†]Presently on sabbatical leave at the Instituto de Ciencias de Materiales de Madrid, Consejo Superior de Investigaciones Científicas, Cantoblanco, 28049 Madrid, Spain.

¹D. Bimberg, M. Grundmann, and N. N. Ledentsov, *Quantum Dot Heterostructures* (Wiley, Chichester, 1998).

²R. A. Masut, C. A. Tran, M. Beaudoin, and R. Leonelli, *Proc. SPIE* **2398**, 116 (1995).

³C. Paranthoen, N. Bertu, O. Dehaese, A. L. Corre, J. Even, S. Loualiche, F. Lissilour, G. Moreau, and J.-C. Simon, *Semicond. Sci. Technol.* **17**, L5 (2002).

⁴P. Miska, C. Paranthoen, N. Bertu, J. Even, O. Dehaese, H. Folliot, N. Bertu, S. Loualiche, M. Senes, and X. Marie, *Semicond. Sci. Technol.* **17**, L63 (2002).

⁵S. Fafard, J. P. McCaffrey, Y. Feng, C. N. Allen, H. Marchand, L. Isnard, P. Desjardins, S. Guillon, and R. A. Masut, *Proc. SPIE* **3491**, 271 (1998).

⁶M. Gendry *et al.*, *J. Appl. Phys.* **95**, 4761 (2004).

⁷N. Shtinkov, V. Donchev, K. Germanova, and H. Kolvev, *Semicond. Sci. Technol.* **15**, 946 (2000).

⁸J. G. Menchero, B. Koiller, and R. B. Capaz, *Phys. Rev. Lett.* **83**, 2034 (1999).

⁹P. J. Poole, J. McCaffrey, R. L. Williams, J. Lefebvre, and D. Chithrani, *J. Vac. Sci. Technol. B* **19**, 1467 (2001).

¹⁰B. Jusserand and M. Cardona, in *Light scattering in Solids V*, edited by M. Cardona and G. Guntherodt (Springer-Verlag, Berlin, 1989).

¹¹B. Jusserand and J. Sapriel, *Phys. Rev. B* **24**, 7194 (1981).

¹²B. Jusserand and D. Paquet, *Phys. Rev. Lett.* **56**, 1752 (1986).

¹³L. Pavesti, G. Mariotto, J. F. Carlin, A. Rudra, and R. Houdré, *Semicond. Sci. Technol.* **9**, 256 (1994).

¹⁴C. A. Tran, J. L. Brebner, R. Leonelli, M. Jouanne, and R. A. Masut, *Phys. Rev. B* **49**, 11268 (1994).

¹⁵J. Groenen, A. Mlayah, R. Carles, A. Ponchet, A. LeCorre, and S. Salaun, *Appl. Phys. Lett.* **69**, 943 (1996).

¹⁶L. G. Quagliano, B. Jusserand, and D. Orani, *Phys. Rev. B* **56**, 4919 (1997).

¹⁷C. A. Tran, R. A. Masut, P. Cova, and J. L. Brebner, *Appl. Phys. Lett.* **60**, 589 (1992).

¹⁸D. Frankland, R. A. Masut, and R. Leonelli, *J. Vac. Sci. Technol. A* **20**, 1132 (2002).

¹⁹P. F. Fewster and C. J. Curling, *J. Appl. Phys.* **62**, 4154 (1987).

²⁰D. Y. Oberli, G. Bohm, G. Weimann, and J. A. Brum, *Phys. Rev. B* **49**, R5757 (1994).

²¹K. J. Jin, S. H. Pan, and G. Z. Yang, *Phys. Rev. B* **50**, 8584 (1994).

²²B. Babic and C. Schonenberger, *Phys. Rev. B* **70**, 195408 (2004).

²³S. Glutsch, D. S. Chemla, and F. Bechstedt, *Phys. Rev. B* **51**, 16885 (1995).

²⁴M. V. Klein, in *Light scattering in Solids I*, edited by M. Cardona (Springer-Verlag, Berlin, 1983).

²⁵W. Hayes and R. Loudon, in *Scattering of Light by crystals*, edited by M. Cardona and G. Guntherodt (Wiley, New York, 1978).

²⁶A. K. Sood, J. Menendez, M. Cardona, and K. Ploog, *Phys. Rev. Lett.* **54**, 2111 (1985).

²⁷B. Jusserand, D. Paquet, and A. Regreny, *Phys. Rev. B* **30**, R6245 (1984).

²⁸A. S. Barker, Jr., J. L. Merz, and A. C. Gossard, *Phys. Rev. B* **17**, 3181 (1978).

²⁹A. J. Shields, M. P. Chamberlain, M. Cardona, and K. Eberl, *Phys. Rev. B* **51**, 17728 (1995).

³⁰*Numerical Data and Functional Relationships in Sciences and Technology*, edited by O. Madelung and H. Weiss, Landolt-Börnstein New Series, Group III, Vol. 17 (Springer-Verlag, Berlin, 1987).

- ³¹P. Hohenberg and W. Kohn, Phys. Rev. **136**, B864 (1964).
³²W. Kohn and L. J. Sham, Phys. Rev. **140**, A1133 (1965).
³³X. Gonze *et al.*, Comput. Mater. Sci. **25**, 487 (2002).
³⁴WWW.abinit.org
³⁵J. P. Perdew and A. Zunger, Phys. Rev. B **23**, 5048 (1981).
³⁶N. Troullier and J. L. Martins, Phys. Rev. B **43**, 1993 (1991).
³⁷H. J. Monkhorst and J. D. Pack, Phys. Rev. B **13**, 5188 (1976).
³⁸J. Moreno and J. M. Soler, Phys. Rev. B **45**, 13891 (1992).
³⁹C. Broyden, Math. Comput. **13**, 577 (1997).
⁴⁰X. Gonze, Phys. Rev. B **55**, 10337 (1997).
⁴¹X. Gonze and C. Lee, Phys. Rev. B **55**, 10355 (1997).
⁴²R. Carles, N. Saint-Cricq, J. B. Renucci, M. A. Renucci, and R. J. Nicholas, J. Phys. C **13**, 899 (1980).
⁴³R. Perez-Alvarez, F. Garcia-Moliner, V. R. Velasco, and C. Trallero-Giner, J. Phys.: Condens. Matter **5**, 5389 (1993).
⁴⁴C. Trallero-Giner, F. Garcia-Moliner, V. R. Velasco, and M. Cardona, Phys. Rev. B **45**, 11944 (1992).
⁴⁵S. F. Ren, D. Lu, and G. Qin, Phys. Rev. B **63**, 195315 (2001).
⁴⁶L. Gonzalez, J. M. Garcia, R. Garcia, F. Briones, J. Martinez-Pastor, and C. Ballesteros, Appl. Phys. Lett. **76**, 1104 (2000).